Nuclear Physics A453 (1986) 189–219

HOT NUCLEAR MATTER IN AN EXTENDED BRUECKNER APPROACH*

A. LEJEUNE

Université de Liège, Institut de Physique au Sart Tilman, B.5, B-4000 Liège 1, Belgium and CRN, F-67037 Strasbourg, France

P. GRANGE and M. MARTZOLFF

CRN and Université Louis Pasteur, F-67037 Strasbourg Cedex, France

J. CUGNON

Université de Liège, Institut de Physique au Sart Tilman, B.5, B-4000 Liège 1, Belgium

Received 20 November 1985

Abstract: The properties of cold and hot nuclear matter are studied in the frame of the Brueckner theory, extended to finite temperature. The basic task is the evaluation of the two-hole line diagram using the Paris potential supplemented by the introduction of three-body forces, coming from the exchange of π and ρ mesons. The latter have an important saturating effect, but not sufficient to reach correct saturation. The latter is achieved by a phenomenological treatment. The properties of hot nuclear matter, for temperatures around 10 MeV, are investigated. Particular attention is paid to one-body properties. The density and temperature dependence of many quantities, like the single-particle energy spectrum, the optical potential, the effective mass, the non-locality of the single-particle field, the mean free path, is displayed and analyzed. The relative importance of the temperature dependence of the g-matrix and of phase space is investigated, especially in relation with the imaginary part of the optical potential and the mean free path. The temperature dependence of the effective mass is particularly studied. It is shown that the peak due to the so-called core polarization effect disappears rapidly as the matter is heated. The evaluation of the entropy and of the level density parameter a, which are closely related, is discussed, and the failure of the Hartree–Fock approach to reproduce the value of a correctly is explained. Two-body properties are also investigated. The temperature and density dependence of the two-body correlations are displayed. Particular attention is paid to the temperature dependence of the effective interaction. The latter is exhibited in a simple manner. It is shown that the effective force felt by low-energy nucleons does not change by more than a few percent when the temperature goes from 0 to 10 MeV. For high-energy nucleons, the change may be as large as ten percent.

1. Introduction

Heavy ion experiments have given rise to an increasing interest in the properties of excited nuclei and of excited nuclear matter. In the course of such reactions, the matter is compressed and excited. In the so-called high-energy domain, the activity during the past ten years has been concentrated on an effort to disentangle between the properties of the excited matter and the mechanism of the reaction, which may

* Work supported by the NATO research grant no 025.81.

very well be such that the first feature is largely masked [1]). Recent developments, however, suggest the possible manifestation of a very hard nuclear matter equation of state between $\sim 2\rho_0$ and $\sim 4\rho_0$, where ρ_0 is the ordinary nuclear matter density [2]). The heavy ion reactions at intermediate energy deal with another aspect of thermal nuclear physics, namely the problem of the maximum excitation energy that a nucleus can withstand. A commonly accepted view [3]) is that below some critical excitation energy, the nucleus remains a somewhat extended system, dissipating its excitation through the evaporation of a few particles. Above the critical excitation, the nucleus disintegrates quickly into many small pieces: the so-called multifragmentation. The critical excitation energy is correlated with the properties of hot nuclear matter, although it probably depends to a large extent on the surface properties and on the Coulomb energy [4]). The manifestation of the multifragmentation in the experimental results is currently investigated [5]).

The general thermodynamical properties of nuclear matter in the domain relevant to intermediate energy heavy ion experiments (i.e. for densities around and below ρ_0, and for temperatures T of a few MeV) are rather well known. Nuclear matter behaves like a van der Waals fluid, with a critical point lying around $\sim \frac{1}{2}\rho_0$, $T \sim$ 10–20 MeV. This results from microscopic calculations using phenomenological interactions [6-7]) as well as from realistic interactions [8-12]). The most advanced works in this second category are the one by Friedman and Pandharipande [10]), using a variational approach with potential forces and the recent works (limited at zero temperature, however) of Anastasio *et al.* [11]) and of Machleidt and Brockmann [12]), based on a relativistic formalism including mesonic forces.

We want here to go back to the problem of cold as well as excited nuclear matter in the frame of an alternative framework, which has proven to be very fruitful in the past: the Brueckner theory. Efforts in this direction have already been made but, in our opinion at least, they appear limited either in their use of simple forces [9]), or in their treatment of the auxiliary potential [8]). Both for cold and hot nuclear matter, our central task has been to calculate the two-hole line diagram, pushing the sophistication as far as we could. Staying in the context of potential forces, we used the Paris potential [13]) and genuine three-body forces. We report here on this calculation and discuss the saturation properties of cold nuclear matter. For hot nuclear matter, we concentrate on single-particles properties (single-particle potential, effective mass, mean free path, ...) rather than on thermodynamical properties (isotherms). We discuss extensively the temperature and density dependence of these various quantities. They are very important in connection with transport properties, especially with thermalization. We also investigate two-body properties like the correlation function and the effective interaction. For the latter, we establish that its temperature dependence is weak, which strengthens the conclusion of ref. [14]).

This paper is organized as follows. In sect. 2, we establish our notation and discuss the saturation curve for cold nuclear matter. We point out the importance of three-body forces. In sect. 3, we present the general framework for studying the

thermodynamics of nuclear matter and present our approximation scheme. We point out the problems raised by this scheme. The latter have often been overlooked in the past. Sect. 4 is devoted to the study of the single-particle spectrum and of the optical potential. Other single-particle properties are investigated in sect. 5. Calculations of the effective mass and of the mean free path are presented. We also show that calculating the entropy within our approximate scheme is bound to fail and that this statement applies to many works based on single-particle approximations. Sect. 6 deals with two-body properties. The temperature dependence of the effective interaction is particularly investigated. The two-body correlations are exhibited under the form of the two nucleon correlated wavefunction. For many of the quantities under investigation, the temperature and the energy dependences are displayed and analyzed. Finally, sect. 7 contains a discussion of our results and our conclusion.

2. The saturation curve

We first establish our notation. The central quantity is the second order term in the hole-line expansion in Brueckner theory, often denoted BB2. We explicitate the occupation numbers, anticipating on sect. 3, where these numbers take values between 0 and 1. The quantity BB2 represents in lowest order in the number of hole lines the energy per nucleon [15])

$$\mathrm{BB2}=\left\{\sum_{k} n(k)\right\}^{-1}\left\{\sum_{k} n(k)\frac{\hbar^2k^2}{2m}+\tfrac{1}{2}\sum_{k,l} n(k)n(l)\langle\widetilde{kl}|g[e(k)+e(l)]|\widetilde{kl}\rangle\right\}, \tag{2.1}$$

where $n(k)$ is the occupation probability for the level of momentum k and where g is the Brueckner reaction matrix [16]), defined by

$$g(w)=v+v\sum_{a,b}\frac{|ab\rangle Q(a,b)\langle ab|}{w+i\varepsilon-e(a)-e(b)}g(w)\,. \tag{2.2}$$

The wiggle in eq. (2.1) indicates that the matrix element is antisymmetrized. The Pauli operator writes

$$Q(a,b)=(1-n(a))(1-n(b))\,. \tag{2.3}$$

The infinitesimal quantity $i\varepsilon$ accounts for the proper boundary condition of the two-nucleon scattering problem associated with the g-matrix [15]). It ensures purely outgoing scattering waves for an initial plane wave. Finally, the single-particle energy $e(k)$ is defined by

$$e(k)=\frac{\hbar^2k^2}{2m}+\mathrm{Re}\;U(k)\,, \tag{2.4}$$

where the average complex field is [15])

$$U(k)=\sum_{j} n(j)\langle\widetilde{kj}|g[e(k)+e(j)]|\widetilde{kj}\rangle\,. \tag{2.5}$$

At zero temperature, the occupation number is simply $n(k)=1$ for $k \leqslant k_F$ and 0 otherwise, and the Fermi momentum k_F is related to the particle number density ρ by the usual relation

$$\rho = \frac{2}{3\pi^2} k_F^3 . \tag{2.6}$$

In this case, the problem amounts to solve eqs. (2.2), (2.4), and (2.5) self-consistently.

Here, while still determining the energy per nucleon in lowest order only in the number of hole lines, we extend the approach by allowing for the presence of three-body forces. It is well recognized that three-body forces are physically relevant in the nuclear context. It is also a well established fact that all nonrelativistic nuclear matter calculations with realistic two-body forces alone are unable to reproduce the empirical binding energy at the proper saturation density [17]). The two-body force that we use here, namely the Paris potential, which however incorporates one-pion and two-pion exchanges on the most satisfying microscopic level, does not escape from this plague. Willing to stay in a nonrelativistic framework the three-body forces have been envisaged as a suitable way to cure this general disease [17-20]). However, only the long range part of the three-body forces, arising from boson exchanges between three nucleons, where one of the nucleons can be excited to a Δ-resonance in the intermediate states, can be handled with detail. Already the $\boldsymbol{L} \cdot \boldsymbol{S}$ component arising from ρ-exchange is of tremendous complexity and therefore is often neglected. The introduction of these three-body forces provides a strong although non sufficient saturating effect, when using realistic ρNN and ρNΔ couplings [21]). It is therefore tempting, and it is the attitude we will adopt here, to assign the (small) lack of saturation to the missing $\boldsymbol{L} \cdot \boldsymbol{S}$ component of the three-body force and include it without further justification in a phenomenological term, which can also stand for other neglected effects, like other (short-range) three-body forces, three-body correlations, ...

The three-body force of ref. [21]) that we consider here arises from 2π, $\pi\rho$ and 2ρ exchange between three nucleons. More elaborate three-body forces exist, but we adopt the model of ref. [21]), because it is in keeping with the boson exchange aspect of the Paris potential. In eq. (2.2), v has thus been split into

$$v = v_2 + v_3 , \tag{2.7}$$

where v_2 is the Paris potential, and where v_3 is the effective two-body forces, coming from integrating one of the nucleon degrees of freedom out of the genuine three-body force W_3:

$$v_3(r_{12}) = \rho \int W_3(r_1, r_2, r_3) g(r_{13}) g(r_{23}) \, \mathrm{d}^3 r_3 . \tag{2.8}$$

In this equation, ρ is the particle density and $g(r)$ is taken as

$$g(r) = (1 - \eta(r))^2 , \tag{2.9}$$

where η is the average s-wave defect function [22]). We thus restrict ourselves to an approximate scheme for the three-body correlated state (in eq. (2.8)) and consider that the most important two-body correlations appear in the $^1S_0$ and $^3S_1$ channels. In this case, v_3 can be written as

$$v_3(r_{12}) = \tau^1 \cdot \tau^2[\sigma^1 \cdot \sigma^2 V_c(r_{12}) + S_{12} V_T(r_{12})], \tag{2.10}$$

with standard notation. In nuclear matter, this force is repulsive and its intensity increases with density. It is rather strongly dependent upon the ρ-coupling constants. Here we choose the so-called strong coupling case with form factor IV as described and discussed in ref. [21]).

In full generality, eq. (2.8) requires v_3 to be calculated at each step of the self-consistency process on the single-particle energies (2.4). Taking advantage of the fact that v_3 adds only a perturbative correction [21]) to the main contribution due to v_2 and of the ultimate phenomenological renormalization just mentioned above we only calculate first and self-consistently the g-matrix with v_2 alone. Therefore we obtain the defect function $\eta(r)$ and compute the value of v_3 with the help of

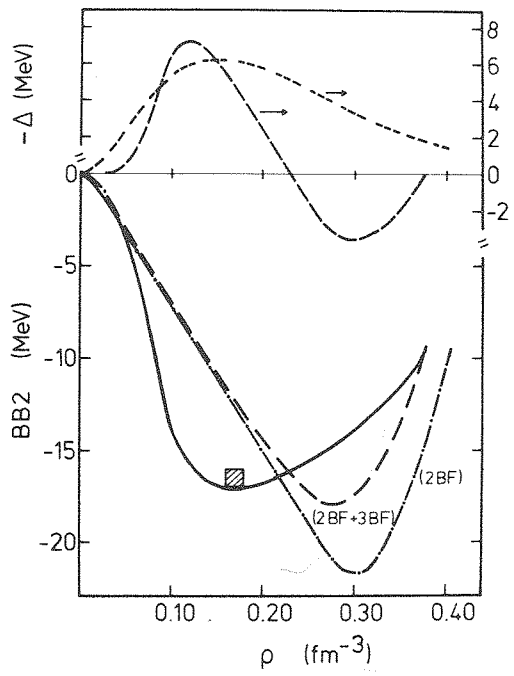

Fig. 1. Lower part: calculated binding energy per nucleon (eq. (2.1)) for cold nuclear matter. The dash-dotted curve corresponds to the two-body interaction (Paris potential) only. The long-dashed curve results from the addition of the three-body forces of ref. [21]). The full curve is obtained after the introduction of the phenomenological correction Δ, as explained in the text. The shape of Δ is represented in the upper part of the figure (scale on the right) by the long-dashed curve. For comparison, the values of Δ adopted in ref. [10]) are given by the short dashed curve.

eq. (2.8). Keeping v_3 unchanged we recalculate self consistently the g-matrix for the full interaction v of eq. (2.7). This is done for every density. Furthermore, we anticipate on the next sections and mention that we neglect the temperature dependence of the three-body force.

The use of a velocity-dependent force, like the Paris potential, introduces a complication in solving the Bethe-Goldstone equation (eq. (2.2)) as compared to the case of a static force and a dramatic lengthening of the numerical calculations. We present several technical aspects in appendix A.

The saturation curve is given by fig. 1. When the Paris potential is taken alone, the corresponding BB2 term gives too strong a binding energy at too large a saturation density, in overall agreement with those of ref. [23]). The introduction of the three-body force as described above improves noticeably the saturation properties, but the saturation still occurs at a too large density. As in ref. [10]), we observe that the long-range $l = 0$ three-body force is not sufficient to ensure saturation properly. This can be done by introducing phenomenologically the contribution due to higher order terms and to the remaining three-body forces. As in ref. [10]), we have added a contribution Δ, the form of which (with the opposite sign) is shown at the top of fig. 1. It has been fitted to reproduce standard saturation properties and compression modulus. The corresponding term used in the variational approach of ref. [10]) is also shown in fig. 1 (upper short-dashed curve), for the sake of comparison. Although they are not very much different, we need some extra repulsion at moderate ($\rho \approx 1.5\ \rho_0$) density to pull the saturation point toward the correct saturation density.

3. Thermodynamics

3.1. GENERAL CONSIDERATIONS

The basic quantity in statistical physics of extended systems is the grand partition function

$$\mathscr{Z} = \langle \exp\left[-\beta(H - \mu N)\right] \rangle , \tag{3.1}$$

where the brackets indicate the average over the grand canonical ensemble in the thermodynamical limit, β is the inverse temperature, μ is the chemical potential, H is the hamiltonian of the system and N is the particle number operator. If H can be split into

$$H = H_0 + H' , \tag{3.2}$$

where H_0

$$H_0 = \sum_k e(k) a_k^+ a_k \tag{3.3}$$

is a single-particle hamiltonian, and where H' is a two-body operator, one can write

$$\ln \mathscr{Z} = \ln \mathscr{Z}_0 - \beta W_L . \tag{3.4}$$

In this relation, $\mathscr{Z}_0$ is the grand partition function associated with H_0 and W_L is the sum of all linked cluster diagrams in a perturbation series in H' at finite temperature [24]). For a non singular interaction, W_L is to first order in H'

$$W_L = \frac{\nu}{2}\int \frac{d^3k}{(2\pi)^3}\int \frac{d^3k'}{(2\pi)^3} n(k)n(k')\langle \boldsymbol{k}\boldsymbol{k}'|H'|\widetilde{\boldsymbol{k}\boldsymbol{k}'}\rangle , \tag{3.5}$$

where $n(k)$ is the usual occupation number probability in the non-interacting limit

$$n(k) = \frac{1}{1+\exp\left[\beta(e(k)-\mu)\right]}, \tag{3.6}$$

and where ν denotes the (spin-isospin) degeneracy of the states $\boldsymbol{k}$. The pressure and particle density are given by

$$p = \nu\frac{T}{2\pi^2}\int_0^\infty dk\, k^2 \ln\left\{1+\exp\left[-\beta(e(k)-\mu)\right]\right\} - W_L , \tag{3.7}$$

or, by partial integration

$$p = \frac{\nu}{2\pi^2}\int_0^\infty dk \frac{k^3}{3} n(k)\frac{de(k)}{dk} - W_L , \tag{3.8}$$

$$\rho = \frac{\nu}{2\pi^2}\int_0^\infty dk\, k^2 n(k) - \left(\frac{\partial W_L}{\partial \mu}\right)_T , \tag{3.9}$$

respectively. The free energy, the entropy and the internal energy per particle are given by

$$\frac{F}{A} = \rho^{-1}\left\{\frac{\nu}{2\pi^2}\int_0^\infty dk\, k^2 n(k)\left[\rho\mu - \frac{k}{3}\frac{de(k)}{dk}\right] + W_L - \mu\left(\frac{\partial W_L}{\partial \mu}\right)_T\right\}, \tag{3.10}$$

$$\frac{S}{A} = \rho^{-1}\left\{-\frac{\nu}{2\pi^2}\int_0^\infty dk\, k^2[n(k)\ln n(k) + (1-n(k))\ln(1-n(k))] - \left(\frac{\partial W_L}{\partial T}\right)_\mu\right\}, \tag{3.11}$$

$$\frac{U}{A} = \rho^{-1}\left\{\frac{\nu}{2\pi^2}\int_0^\infty dk\, k^2 n(k)e(k) + W_L - T\left(\frac{\partial W_L}{\partial T}\right)_\mu - \mu\left(\frac{\partial W_L}{\partial \mu}\right)_T\right\}, \tag{3.12}$$

respectively.

The perturbation expansion of W_L in terms of a regular interaction can be found in many standard textbooks. For a singular interaction, the problem has not been very much studied (in ref. [8]) e.g., the problem is avoided, and the most obvious modification, due to the "heating" of the Pauli principle is taken for granted). The standard Bethe-Brueckner resummation of the ladder diagrams into a g-matrix can of course be done at finite temperature. In this case, it is easy to see [24]) that the g-matrix obeys eq. (2.2), with a Pauli operator (2.3) containing occupation number of the type (3.15), which now differ from 0 and 1. In this case, the two-hole line diagram is of the form usually assumed [8-9]).

The hamiltonian H_0 in eq. (3.2) may be chosen to include the average potential as defined by eq. (2.5) for any state. This choice preserves at finite temperature the usual cancellation between diagrams containing potential insertions and those containing bubble insertions to the lowest order. The perturbation series of W_L at $T \neq 0$ includes terms [24]) not present at $T = 0$, but with the above single-particle choice, the contribution up to the two-hole line diagram keeps the same structure. In this approximation, W_L writes

$$W_L = -\frac{\nu}{2} \int \frac{d^3k}{(2\pi)^3} \int \frac{d^3k'}{(2\pi)^3} n(k) n(k') \operatorname{Re} \langle \boldsymbol{k}\boldsymbol{k}' | g[e(k) + e(k')] | \widetilde{\boldsymbol{k}\boldsymbol{k}'} \rangle . \quad (3.13)$$

The real part is introduced to guarantee real values to the physical quantities (3.10)-(3.12). The complex character of g is coming from the choice of the single-particle potential. The whole perturbation series of W_L should in principle be independent of this choice and thus be real, but any truncation will give a complex result. The imaginary part of $e(k)$ has obvious physical meaning, but the imaginary part corresponding to (3.13) has not. In conclusion, up to the two-hole lines contribution, the general structure of the Brueckner theory is preserved after the proper modification of the quantities $n(k)$.

3.2. APPROXIMATION SCHEME

The calculation of all the quantities (3.7)-(3.12) could in principle be done starting from given values of μ and T. However, doing so, we observed that the self-consistency on $e(k)$, which defines $n(k)$ at every step, may never be achieved for some values of μ and T. The calculation shows an instability in the density, which becomes smaller and smaller at each iteration. In our opinion, this instability is probably related to the underlying instability of the van der Waals type. In view of this situation, one would be inclined to use the density as an input instead of the chemical potential. This is feasible if the second term in eq. (3.9) is neglected. In this case, we write

$$\rho = \nu \int \frac{d^3k}{(2\pi)^3} n(k) , \quad (3.14)$$

with

$$n(k) = \frac{1}{1 + \exp[\beta(e(k) - \tilde{\mu})]} . \quad (3.15)$$

In this scheme, $\tilde{\mu}$ looses its status of chemical potential (see below) and eqs. (3.14)-(3.15) should be considered as a suitable description of the one-body density. From ρ and T, one can extract the value of $\tilde{\mu}$, and so determine the $n(k)$ and calculate other quantities. The inversion of eq. (3.9) to determine μ from ρ and T, even with the simplest approximation of W_L is technically impossible. In keeping

with the neglect of the derivative of W_L in eq. (3.9), we neglect the derivatives of W_L everywhere. Actually, we calculate the internal energy by

$$\frac{U}{A}=\rho^{-1}\left\{\frac{\nu}{2\pi^2}\int_0^\infty \mathrm{d}k\, k^2 n(k)e(k)+W_L\right\}, \tag{3.16}$$

with W_L given by eq. (3.13). In summary, eqs. (3.14)-(3.16), (3.13) and (2.2)-(2.5) constitute our approximation scheme.

3.3. CONSERVING AND NON-CONSERVING APPROXIMATIONS

From the general thermodynamical relation

$$p=\rho^2\left(\frac{\partial(F/A)}{\partial\rho}\right)_T=\rho\left(\mu-\frac{F}{A}\right), \tag{3.17}$$

one can deduce that, for an extended system at equilibrium ($p=0$), one has

$$\mu=\frac{F}{A}. \tag{3.18}$$

This is the expression of the Hugenholtz-Van Hove theorem [25]). It turns out, that numerically, $\tilde{\mu}$ is different from F/A, which signals as we said above, that it lost the meaning of a chemical potential. In other terms, our approximation is not conserving. To discuss this point further, one may consider the pressure, the density and the free energy per particle, given respectively by eqs. (3.7), (3.9), and (3.10), as three functions of two parameters μ and T

$$p=p(\mu, T), \tag{3.19a}$$

$$\rho=\rho(\mu, T), \tag{3.19b}$$

$$F/A=F/A(\mu, T). \tag{3.19c}$$

Therefore, they are linked by some relation. The latter is usually formulated as either

$$p=\rho\left(\frac{F}{A}-\mu\right), \tag{3.20}$$

or

$$p=\rho^2\left(\frac{\partial(F/A)}{\partial\rho}\right)_T. \tag{3.21}$$

An approximation scheme replaces the functions p, ρ, and F/A in eqs. (3.19) by some approximate ones. The relation (3.20) (or (3.21)) is then no longer guaranteed. It is indeed not fulfilled in our approximation scheme. The non-conserving character of the latter arises from the neglect of the second term in eq. (3.9). Any approximation on W_L will be conserving if it is taken the same in eqs. (3.7), (3.9) and (3.10). This

problem has received attention in ref. [15]), for $T=0$. Therein, it is shown that our approximation scheme can be made practically conserving, if the chemical potential μ is derived from the parameter $\tilde{\mu}$ by

$$\mu = \tilde{\mu} - \frac{1-\zeta}{2-\zeta} \operatorname{Re}\, U(k)|_{e(k)=\tilde{\mu}}\,, \tag{3.22}$$

where

$$\zeta = 2 - \frac{\overline{m_1}}{m}\,. \tag{3.23}$$

In this relation, $\overline{m_1}$ is the E-mass (see ref. [15]) and later) and where the overall bar means an average value over the occupied states.

In view of the above discussion, the difficulty can be turned in the following way. We evaluate U/A as discussed in sect. 3.2. The free energy F/A is calculated using the single-particle value of the entropy (eq. (3.11) when the last term is dropped), and the pressure is calculated by relation (3.21). The conserving character of eq. (3.22) has been checked by recalculating the pressure by eq. (3.7) with μ given by eq. (3.22) and W_L evaluated as for U/A. Both procedures agree reasonably well.

It is remarkable that the non-conserving character of our approximation scheme arises from the necessary self-consistency of the Brueckner g-matrix. Indeed, the Hartree-Fock scheme for an effective (non-singular) Skyrme interaction, which

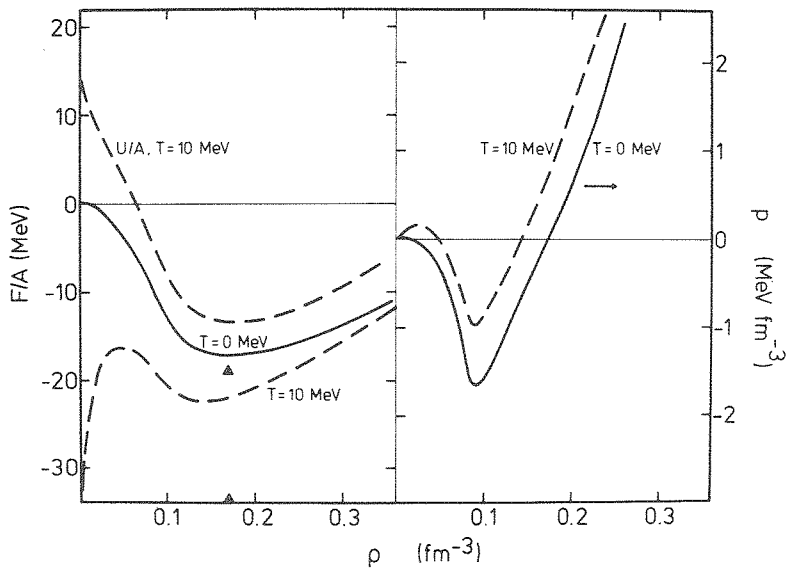

Fig. 2. The left-hand part gives our predictions for the nuclear matter internal energy (two upper curves) and free energy (lower curve) per nucleon. The triangles show the value of the free energy per nucleon for $\rho=\rho_0$, and $T=8$ MeV and $T=20$ MeV, respectively. The right-hand part gives the $T=0$ and $T=10$ MeV isotherms, as calculated by eq. (3.21). See text for detail.

presents the same structure as our approximate scheme, turns out to be perfectly conserving [26]).

3.4. RESULTS

Typical results are contained in fig. 2. The phenomenological correction for the short-range three-body force introduced in fig. 1 is also included here and kept the same irrespective of the temperature. The isotherms shown on the right part of the figure are calculated as explained in sect. 3.3. Nothing unexpected arises from the results and all trends agree more or less with phenomenological [6,7]) or variational [10]) calculations. The only noticeable difference is that we obtain (in absolute value) larger pressure. To know whether this comes from some features of the theory or of the forces or simply from our approximation scheme deserves further work. The huge cost of the calculation (see appendix A) prevented us to go further. We therefore prefer to focus on the single-particle properties in the next sections.

4. The single-particle spectrum

We recall that the quantity $U(k)$ is complex. Its real part can be considered as the average potential felt by a nucleon of momentum k. In fig. 3, Re $U(k)$ is displayed for several densities, both at $T=0$ and at $T=10$ MeV. One can also read from this figure the effect of the three-body force at $T=0$. As expected, their main effect is to make the real part of the average potential less attractive for the most important values of the momentum k. This is in keeping with their repulsive effect on the average binding energy. However, for large k, the effect is reversed, a feature which is not intuitively understandable. However, we have observed in many cases that the modification of the low momentum part of the energy spectrum is correlated to the modification of the high momentum part, because of the non linearities introduced by the energy denominators of the g-matrix.

The depth of the real potential is increasing with density, for low momentum. On the other hand, it is more and more repulsive for high momentum. This would indicate that the balance between the attractive and repulsive forces is in favour of the attractive ones at low momentum and in favour of the repulsive parts at high momentum (larger than about twice the Fermi momentum). We will come back on this point.

The temperature dependence of the single-particle field $U(k)$ is sketched in fig. 3. At density between $\sim 0.17\ \mathrm{fm}^{-3}$ and $0.33\ \mathrm{fm}^{-3}$, the main effect is a reduction of the attractive mean field as the temperature increases. At small densities, the situation is somewhat different, since an increase of the average potential takes place for low momentum. This result can be understood from the following rough picture of the Brueckner reaction matrix. The latter results from a reduction of the attractive force and a renormalization, i.e. a strong reduction of the repulsive force. However,

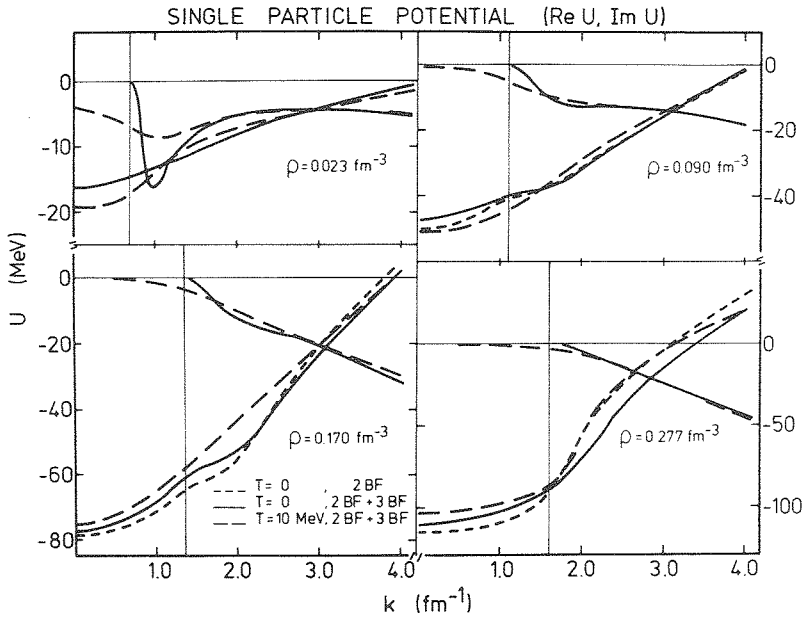

Fig. 3. Calculated values of the single-particle field $U(k)$ inside nuclear matter for several densities, as a function of the nucleon momentum k. The real part of $U(k)$ is given by the bunch of curves going from lower left to upper right in each box. The imaginary part of $U(k)$ is given by the remaining curves. For both quantities, the full lines correspond to $T=0$, and the long dashed curves to $T=10$ MeV. The short dashed curve gives the real part of $U(k)$ at $T=0$, when the three-body forces are removed. See text for detail. The left (right) scale stands for the left (right) part of the figure.

depending upon the situation, the reduction may be more effective for one part than for the other. For instance, at high densities, it is reasonable to consider that the Pauli operator is acting more on the repulsive forces. Therefore, an increase in temperature, leading to a softening of the Pauli operator, gives more importance to the repulsive forces at large densities. On the contrary, at low density, the repulsive forces play a minor role and a softening of the Pauli operator gives rise to an increase of the attractive mean field.

Let us come to the imaginary part of the single-particle field $U(k)$. The latter comes from real excitations induced by a particle created in the heated Fermi sea with momentum k. This requires the promotion of one particle from an occupied orbit to a higher orbit. For the same order in the perturbative expansion as for the real part, the imaginary part of the average potential (2.5) may be written as [15]:

$$\begin{aligned}\text{Im } U(k) = \frac{\pi}{2}\int \frac{\mathrm{d}^3k_1}{(2\pi)^3}\int \frac{\mathrm{d}^3k_2}{(2\pi)^3}\int \frac{\mathrm{d}^3k_3}{(2\pi)^3}\,|\langle \overline{\boldsymbol{k}\boldsymbol{k}_1}|g[e(k)+e(k_1)]|\widetilde{\boldsymbol{k}_2\boldsymbol{k}_3}\rangle|^2 \\ \times n(k_1)(1-n(k_2))(1-n(k_3))\delta(\boldsymbol{k}+\boldsymbol{k}_1-\boldsymbol{k}_2-\boldsymbol{k}_3) \\ \times\delta(e(k)+e(k_1)-e(k_2)-e(k_3))\,, \qquad (4.1)\end{aligned}$$

where we have made explicit the conservation of momentum and energy. If $\langle g \rangle$ denoted a mean value, it can be singled out of the integral and the remaining part is the so-called phase-space integral, which just counts the number of 2p-1h states accessible in accordance with the Pauli principle. Then,

$$\text{Im } U(k) = \frac{\pi}{2}\langle g \rangle \int \frac{\mathrm{d}^3k_1}{(2\pi)^3}\int \frac{\mathrm{d}^3k_2}{(2\pi)^3}\int \frac{\mathrm{d}^3k_3}{(2\pi)^3}\, n(k_1)(1-n(k_2))(1-n(k_3)) \times \delta(\boldsymbol{k}+\boldsymbol{k}_1-\boldsymbol{k}_2-\boldsymbol{k}_3)\delta(e(k)+e(k_1)-e(k_2)-e(k_3))\,. \tag{4.2}$$

At $T=0$, the conservation of energy-momentum forces Im $U(k)$ to vanish below the Fermi level. Close to the Fermi level, the phase-space leads to a quadratic increase of Im $U(k)$ with energy $e(k)$, or with the momentum.

Numerical results are shown in fig. 3. At zero temperature, and for most of the densities investigated here, the imaginary part increases steadily with momentum, but in general in a way which is not following the phase space (eq. (4.2)). The influence of the latter can be identified close to the Fermi momentum. The big bump observable for $\rho = 0.023$ fm^{-3} is also due to the dynamical variation of the g-matrix. Let us remind that the intensity of the imaginary part at low density is generally related to the surface absorption of low energy ($\lesssim$20 MeV) nucleons by atomic nuclei. In contrast to what happens for the real part, the influence of three-body forces turns out to be negligible on the imaginary part and therefore is not displayed in fig. 3.

The temperature dependence of the imaginary part is the strongest at low density. At $\rho = 0.023$ fm^{-3}, there is a dramatic change of Im $U(k)$. The most noticeable feature is, of course, the non-vanishing values below the Fermi momentum k_F, to keep on with this vocabulary at finite temperature. This comes from the partial occupation of levels below k_F, which makes real transitions possible. For the same density, there is a decrease of the imaginary part a little bit above the Fermi level. This seems to be quite general for almost all densities studied here. Such a feature can be understood from fig. 4, which depicts typical 2p-1h configurations. On the left is a 2p-1h configuration which is accessible from $k < k_F$ at $T \neq 0$ and not at $T=0$. On the right, there is a typical 2p-1h configuration accessible from $k > k_F$ (at any T). In eq. (4.1), this configuration is weighted by the factor

$$f = n(k_1)(1-n(k_2))(1-n(k_3))\,. \tag{4.3}$$

At $T=0$, $f=1$, but at $T\neq 0$, the weight is smaller. In a typical situation, $n(k_1)\approx 0.9$, $n(k_2)\approx n(k_3)\approx 0.1$, and therefore, $f\approx 0.7$. So, if the nucleon has a momentum, say between $\sim k_F$ and $\sim 2k_F$, the weight of the intermediate configurations is reduced. This reduction seems to be important enough to counterbalance the opening of the phase space due to the increase of the temperature (part (a) of fig. 4). This is not the only effect, as we will see below.

At large momentum, the phase space is not changed significantly when going from $T=0$ to $T=10$ MeV. As a consequence, the imaginary part is not very much

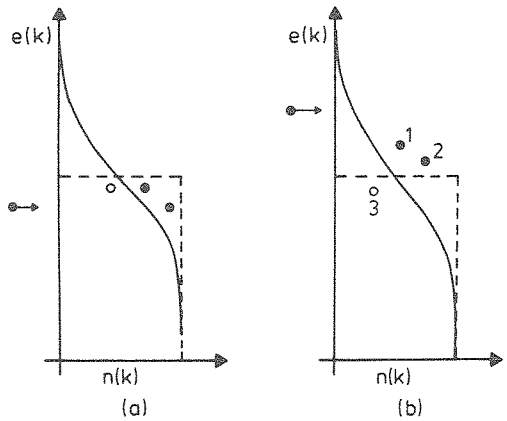

Fig. 4. Typical 2p-1h configurations contributing to the imaginary part of the average single-particle field. In (a), the 2p-1h configuration is irrelevant for $T=0$. See text for discussion.

affected. In short, the temperature dependence of Im $U(k)$, which is due to phase-space modifications is important only when the energy of the nucleon is within T or so off the chemical potential, i.e. the Fermi energy when $T \to 0$.

The temperature dependence also comes from the dynamical features embedded in the g-matrix. The latter is influenced by the temperature dependence of the Pauli operator (eq. (2.3)). To exhibit this effect, we present in fig. 5 the result of a

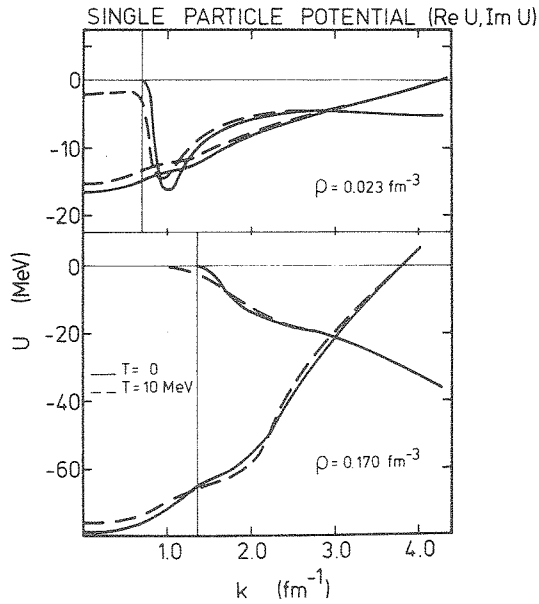

Fig. 5. Same as left-hand part of fig. 3, when the Pauli operator is "frozen". Same conventions are used. See text for detail.

calculation using temperature dependent occupation numbers $n(k)$, everywhere (eqs. (2.1), (2.5)), but not in the Pauli operator (eq. (2.3)): the latter is "frozen". For simplicity, we have disregarded the (unimportant in this case) three-body forces. The variation of the imaginary part of $U(k)$ is qualitatively the same as for the full Pauli operator, but by comparing figs. 3 and 5, it is seen that the "heating" of the Pauli operator results in non negligible effects, for momenta between $\sim k_F$ and $\sim 2k_F$.

There is an intimate connection between the single-particle spectrum and the optical-model potential. We recall that the latter is not simply U as a function of the single-particle energy, as proposed in ref. [27]), but rather [28-30])

$$U_{\text{opt}}(E) = V(E) + iW(E)\,, \tag{4.4}$$

with

$$V(E) = \text{Re}\; U(k(E))\,, \tag{4.5}$$

$$W(E) = \frac{\tilde{m}}{m}\,\text{Im}\; U(k(E))\,. \tag{4.6}$$

In these equations, $k(E)$ is the root of the implicit equation

$$E = \frac{\hbar^2 k^2}{2m} + \text{Re}\; U(k)\,, \tag{4.7}$$

and $\tilde{m}$ is the so-called k-mass (see below). This quantity enters eq. (4.6) because of dispersion effects. Note that E is equal to $e(k)$ for $k = k(E)$.

Calculated values of $V(E)$ are given in fig. 6, both at $T = 0$ and $T = 10$ MeV for several densities. At $T = 0$, the variation with respect to E is typically the same as for a two-body force alone [27]), i.e. a steady increase of the attractive field with the density. Also the manifestation of the repulsion is more apparent at larger density. Let us also notice the sizeable attenuation of the real field for ordinary nuclear matter density when the temperature raised. Finally, at $T = 10$ MeV, a change of sign of the average field still occurs at high energy. The critical energy decreases when the density increases. Therefore, at sufficiently high energy, the real part of the optical potential for nucleon-nucleus scattering (evaluated f.i., in a local density approximation) is still expected to exhibit a wine-bottle bottom shape [31]) at finite temperature.

A parameter linked with the potential $V(E)$ which is often referred to, because it is directly measurable (at least for $T = 0$), is the slope α of the curve $V(E)$ as a function of E. Between ~ 20 MeV and ~ 120 MeV, the latter is roughly linear

$$V(E) \approx V_0 + \alpha E\,. \tag{4.8}$$

In our calculation, $\alpha \approx 0.23$ at normal conditions ($\rho \approx \rho_0$, $T = 0$) and does not change significantly as T increases up to 20 MeV. This rather low value is attributed to three-body forces. When the latter are removed, the value of α is ≈ 0.28, very close to the value obtained with other potentials [27]) and to the experimental value [32]).

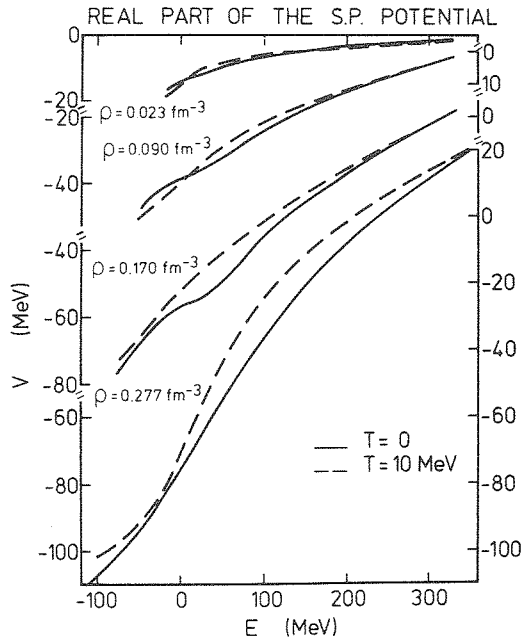

Fig. 6. Calculated real part of the optical potential $V(E)$ (eq. (4.5)) for several nuclear matter densities ρ and for two temperatures ($T = 0$, full curve and $T = 10$ MeV, long dashes), as a function of the nucleon energy E. See text for detail.

Fig. 7 displays the calculated values of $W(E)$ as a function of the energy E (eq. (4.6)) for $T = 0$ and $T = 10$ MeV and for different values of the density. The energy dependence of the imaginary part reflects the k-dependence of Im $U(k)$. In other words, there is practically no distortion coming from the dispersion relation $E = E(k)$ (eq. (4.7)) nor from k-mass $\tilde{m}/m$. Note that, in fig. 7, the $T = 0$ curves stop at the Fermi energy, whereas the $T = 10$ MeV curves stop at the bottom of the Fermi sea, when $k = 0$.

5. Other single-particle properties

5.1. EFFECTIVE MASSES

We briefly review the various effective masses, which are usually considered. The ordinary effective mass m^*/m may be defined as ($\hbar = 1$)

$$\frac{m^*}{m} = \frac{k}{m}\left(\frac{\mathrm{d}e(k)}{\mathrm{d}k}\right)^{-1}. \tag{5.1}$$

It is the product of the k-mass by the E-mass

$$\frac{m^*}{m} = \frac{\tilde{m}}{m} \times \frac{\bar{m}}{m}, \tag{5.2}$$

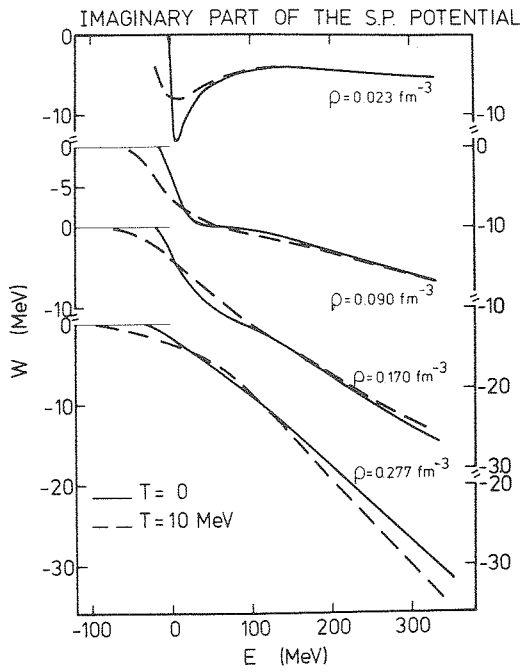

Fig. 7. Same as fig. 6 for the imaginary part $W(E)$ (eq. (4.6)) of the optical potential. See text for detail.

with

$$\frac{\tilde{m}}{m}=\left\{1+\frac{m}{k}\left[\frac{\partial}{\partial k}\,\mathrm{Re}\,M(k,E)\right]_{E=e(k)}\right\}^{-1}, \tag{5.3}$$

and

$$\frac{\tilde{m}}{m}=1-\frac{\partial}{\partial E}\left[\mathrm{Re}\,M(k,E)\right]_{E=e(k)}. \tag{5.4}$$

In this equation $M(k, E)$ is the so-called mass operator, that we have calculated here in the Brueckner-Hartree-Fock approximation

$$M(k,E)=\sum_j n(j)\langle \widetilde{kj}|g[E+e(j)]|\widetilde{kj}\rangle . \tag{5.5}$$

The mass $\tilde{m}$ reflects the non-locality of the average field (see eq. (2.5)). Mainly the latter comes from the antisymmetrization. Moreover for the Paris potential, an additional source of non-locality is due to the momentum dependence of the interaction. In fig. 8, we show our results for the $\tilde{m}$ mass for several densities and for two temperatures $T=0$ and $T=10$ MeV. As expected, the $\tilde{m}$ mass comes closer and closer to unity (no non-locality effect) when the density decreases. At normal nuclear matter density, the mass $\tilde{m}/m$ is around 0.6 for a particle around the Fermi momentum, a result which seems to be rather independent of the dynamics [15]).

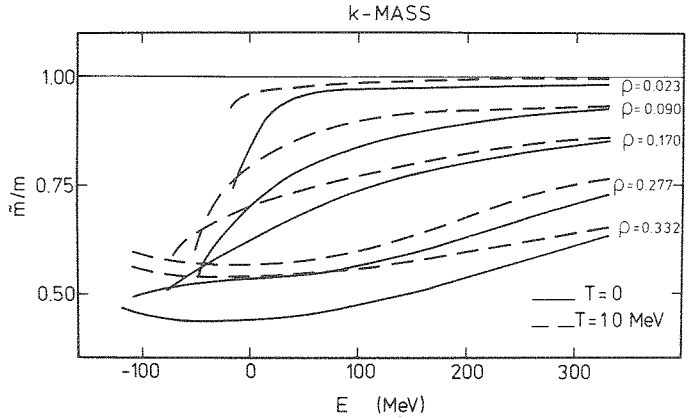

Fig. 8. Calculated values of the k-mass $\tilde{m}/m$ (eq. (5.3)). Same convention as in fig. 6.

When the temperature increases, $\tilde{m}/m$ comes nearer unity, which arises from the fact that the high relative momenta $k-j$ in eq. (5.5) are more and more important, and make the g-matrix vanishingly small.

Let us now turn to the effective mass m^*. The energy and temperature dependence of this quantity is shown in fig. 9, for ordinary nuclear matter density. For cold nuclear matter, the shape of m^*/m as a function of the energy is essentially the same as for other potentials [15]). It exhibits three features: an infinite slope at $k = k_F$, a peak somewhat above the Fermi level, and a kind of raising background underneath. The peak originates from the energy (E)-dependence of the mass operator. Physically, it is due to the low lying core polarized states, which are easily excited by a nucleon of momentum just above k_F [ref. [15])]. Just to connect with the terminology of previous works, the peak corresponds to core polarization effects

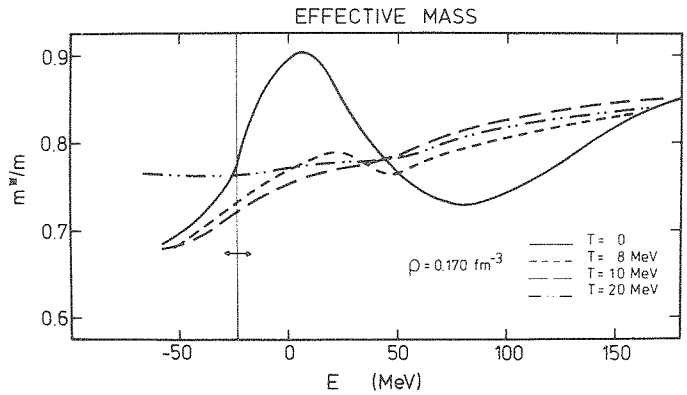

Fig. 9. Calculated values of the nucleon effective mass m^*/m inside nuclear matter at ordinary density. The various curves correspond to the various temperatures indicated in the lower right corner. The arrow gives the values of E, which are relevant for the calculation of the entropy at $T = 10$ MeV. See text for detail.

only. The so-called correlation effects would shift it towards the Fermi momentum, as is well known.

As the temperature increases, the peak in m^* collapses rapidly. This is understandable in view of fig. 4, since the 1p-1h core polarized states can be excited from any single-particle orbit. The perhaps surprising feature is the rapidity of the modification. Already at $T = 8$ MeV, the peak has disappeared. Note that this could have been inferred from fig. 3, since a wiggle in the curve Re $U(k)$ around the Fermi momentum is responsible for a peak in m^*.

The above discussion is also of interest when one reminds of the link between m^* and the level density parameter a. For an extended system, the latter appears as the first coefficient of the usual expansions of the internal energy

$$\frac{U}{A} = \frac{U}{A}(T=0) + \frac{a}{A}T^2 + \cdots \tag{5.6}$$

and of the entropy

$$\frac{S}{A} = 2\frac{a}{A}T + \cdots . \tag{5.7}$$

Starting from the single-particle expression of the entropy (and eq. (3.11) without the last term) and using standard techniques [33]), one readily gets

$$\frac{a}{A} = \frac{1}{3\rho}\left(\frac{m^*}{m}km\right)_{k=k(\mu)} . \tag{5.8}$$

This equation stresses the importance of the effective mass. However, the strong bump present in the function $m^*/m(E)$ (see fig. 9) does not show up directly in the calculation of the entropy. Indeed, at small temperatures, the single-particle entropy depends on k-values very close to the Fermi momentum, as indicated by the arrow in fig. 9. Therefore the effective mass in that case is around 0.75. If the temperature increases, the band of the important k-values broadens, but at the same time, the peak in the function m^* rapidly collapses. Hence the calculated value of the entropy at $T = 8$ MeV divided by the temperature is consistent with the value given by eq. (5.8) with $m^*/m = 0.75^*$. We get $a \approx \frac{1}{19}A$, whereas with Skyrme III, the Hartree-Fock theory gives $a \approx \frac{1}{20}A$. In the latter case, m^*, which is equivalent to $\tilde{m}$, because there is no dynamical energy dependence, is equal to 0.73, very close to the relevant value of m^* at the Fermi level. Eq. (5.8) opens interesting possibilities, however. It has been shown [34]) that further approximations to m^* including correlation effects produce a peak *at* the Fermi level, with a maximum value $m^*/m \approx 1$, in agreement with a previous conjecture of Brown *et al.* [35]). At this level of approximation, a nuclear matter value of $a \approx \frac{1}{14}A$ is obtained. We recall that with a typical effective force like Skyrme III, the level density parameter a, goes from $A/20$ in

* It is not surprising that expression (5.7) is still valid at $T = 8$ MeV. These expansions are essentially expansion in T/ε_F, where ε_F is the kinetic energy of the Fermi level.

nuclear matter to $\sim\frac{1}{15}A$ in finite nuclei. Assuming a change of the same magnitude for a calculation fulfilling $m^*/m \approx 1$ near the Fermi level, a value of a close to the experimental one ($\sim\frac{1}{8}A$) is plausible. This conjecture need however to be checked by further work.

It is interesting to note that our approximation to U/A goes beyond the single-particle picture (without however including correlation effects). Therefore, in this approximation, expansion (5.6) yields another value of a. Straightforward calculations yield

$$\frac{a}{A}=\frac{1}{3\rho}\left\{\frac{m^{*2}}{k}2\left[\frac{k^2}{2m}+\tfrac{1}{2}\,\mathrm{Re}\;U(k)\right]+\frac{m^*}{m}\frac{k}{2}(m+m^*)\right\}_{k=k(\mu)}. \tag{5.9}$$

With our numerical values, one gets in this case $a \approx \frac{1}{18}A$, which is essentially the same as the value quoted above.

5.2. MEAN FREE PATH

The mean free path λ of a nucleon of energy E inside nuclear matter is related to the imaginary part of the optical potential. The mean free path λ is usually defined [15]) as half the inverse of the imaginary part of the momentum $k_R + ik_I$, which satisfies the dispersion relation

$$\frac{\hbar^2}{2m}(k_R+ik_I)^2+U(k_R+ik_I)=E. \tag{5.10}$$

In first approximation k_R is the momentum obeying eq. (4.7), and λ is, using eqs. (4.7), (4.6) and (5.10)

$$\lambda=\frac{\hbar^2 k(E)}{2m}\frac{m}{\tilde{m}}\frac{1}{\mathrm{Im}\;U(k(E))}. \tag{5.11}$$

The quantity λ can be understood as the length parameter governing the exponential decay of a single-particle wavefunction of a nucleon of energy E. In a somewhat familiar picture, it is the average distance that a nucleon has to cover before undergoing an interaction. Another related concept, the thermalization mean free path λ_{th} is the length that a nucleon has to travel before being in equilibrium with the surrounding medium. The two quantities may be roughly related by

$$\lambda_{th}=\lambda\frac{\overline{\Delta k_z}}{k}, \tag{5.12}$$

where $\overline{\Delta k_z}$ is the average longitudinal momentum loss per interaction. The quantity λ_{th} is very important, since it largely controls the thermalization of the matter during heavy ion collisions.

In fig. 10, we report on the calculation of $\lambda(E)$ for several densities and for two temperatures. For cold matter, the mean free path becomes infinite at the Fermi

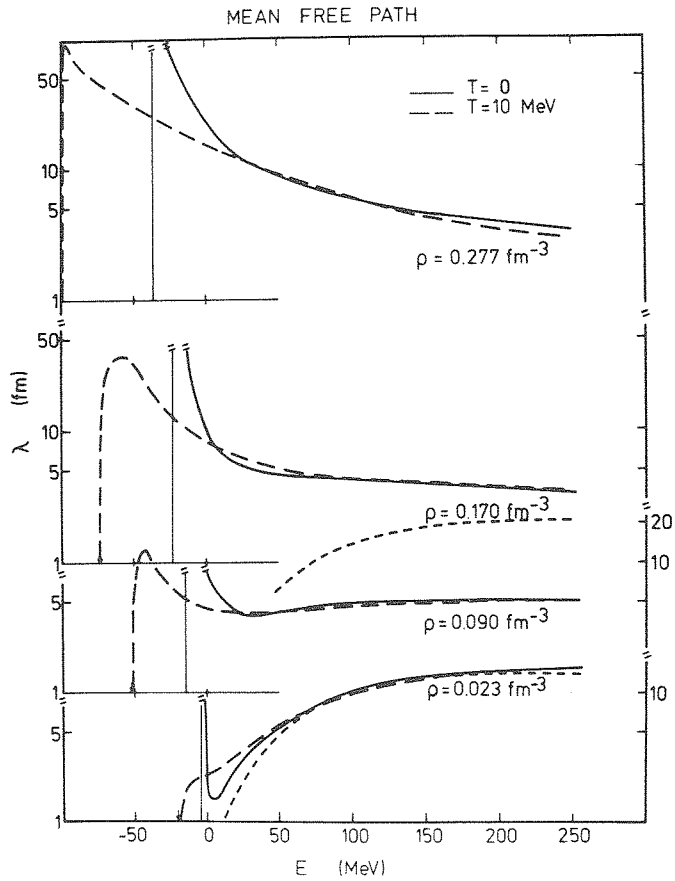

Fig. 10. Predicted values of the nucleon mean free path λ (eq. (5.11)) inside nuclear matter for several densities and for two temperatures ($T = 0$, full curve; $T = 10$ MeV, long dashes). The small dashed curves give the classical value (eq. (5.13)).

momentum because of the Pauli principle which forbids any real transition for a nucleon of that momentum. The classical value of the mean free path (short dashed curve in fig. 10) is

$$\lambda_{\mathrm{cl}} = (\rho\bar{\sigma})^{-1}, \tag{5.13}$$

where $\bar{\sigma}$ is the average of the proton–proton and neutron–proton total cross sections. Using eq. (4.1) and approximating the g-matrix by its mean value $\langle g\rangle$ over phase-space, we can write

$$\lambda = \frac{\hbar^2 k(E)}{2m}\,\frac{m}{\tilde{m}}\,\frac{1}{(\frac{1}{2}\pi)\rho|\langle g\rangle|^2\, Y(E,\rho)}, \tag{5.14}$$

where $Y(E,\rho)$ is the integral appearing in eq. (4.2) and counting the allowed intermediate states. In the very high energy limit or in the dilute limit,

$(\pi m)/(\hbar^2 k(E)|\langle g\rangle|^2)$ tends to the free scattering cross section and $Y \to 1$. Also, in these limits (see fig. 8), $\tilde{m}/m$ is close to unity. Our calculation displays this limiting behaviour for $\rho = 0.023\ \mathrm{fm}^{-3}$ (see fig. 10). The deviation from the classical value (eq. (5.13)) is due to dispersion effects ($\tilde{m}$) or to the Pauli principle, through g, which is different from the free scattering matrix and through Y. Obviously, the divergence close to the Fermi momentum are due to the Pauli blocking of the intermediate states (function Y). As the energy increases, the function Y is becoming less and less important, and the Pauli blocking hidden in the g-matrix is coming more and more into play. Around $E = 200$ MeV and at $\rho = \rho_0$, dispersion effects are not negligible at all. Fig. 8 tells that $\tilde{m}/m \approx 0.80$ and this factor accounts for about half the difference between λ and λ_{cl}. Note the very big effect of the Pauli principle, which is responsible for an *increase* of λ (at least for $E < 100$ MeV) when the density increases, in contrast to a *decrease* of λ_{cl} (eq. (5.13)).

The temperature effects on the mean free path λ are spectacular. Because of the relaxation of the Pauli blocking, the infinities are removed. The mean free path remains quite long however (except for very small densities) when the energy is below the Fermi energy. The vanishing of λ at the very end of the energy scale is just a kinematical effect. For a nucleon at the bottom of the Fermi sea, $k = 0$ and through eq. (5.11), $\lambda = 0$. The decrease of the mean free path for increasing temperature certainly helps to thermalize the nuclear system during heavy ion collisions at intermediate energies [36]).

6. Two-body properties

6.1. THE EFFECTIVE INTERACTION

We want here to examine briefly the important question of the temperature dependence of the effective interaction. The latter can be defined as the g-matrix itself. This quantity is however a function of many variables. In order to have a comprehensive and intuitive picture, it is perhaps more useful to consider averages over some of these variables, retaining only one or two. In many cases [26,37–38]), the effective interaction V_{eff} is conveniently defined by

$$V_{\mathrm{eff}} = -\frac{V(E)}{\rho}, \tag{6.1}$$

where $V(E)$ is the real part of the optical potential (4.5). With the help of eqs. (4.5) and (2.5), it can be seen that the detail of the g-matrix dependence upon the total momentum of two interacting particles and on the relative orientation of the total and relative momenta have been averaged out in eq. (6.1). Furthermore, the absolute value of the relative momentum has been averaged over the Fermi sea. Roughly speaking, V_{eff} represents the average effective interaction acting between a nucleon

of energy E and a nucleon inside the Fermi sea. The results of our calculation are displayed in fig. 11, where V_{eff} is displayed as a function of the density and of the energy of the particles. In the range of the parameters shown, the effective interaction may change by more than 10% when going from $T=0$ to $T=10$ MeV. At low energy however ($E \leqslant 0$), the temperature dependence is smaller, causing at most a 5% effect in the $T=0$–10 MeV range. This property holds for a nucleon inside the Fermi sea, as can be seen from fig. 6. This indicates that typical finite temperature Hartree-Fock calculations of nuclei need not be renormalized, since the Hartree-Fock approximation itself is not expected to be better than these 5%. Our results agree with those of ref. [14]), which addresses to the same problem, but uses a much less sophisticated method and deals with the neutron gas.

6.2. THE CORRELATED WAVEFUNCTION

In relation with the statistical property of an extended system it is important to know how the interactions correlate pairs of particles inside this system. These properties can be expressed, in the frame of the approach adopted here, by the correlated wavefunction, i.e. the wavefunction for the relative motion of two nucleons

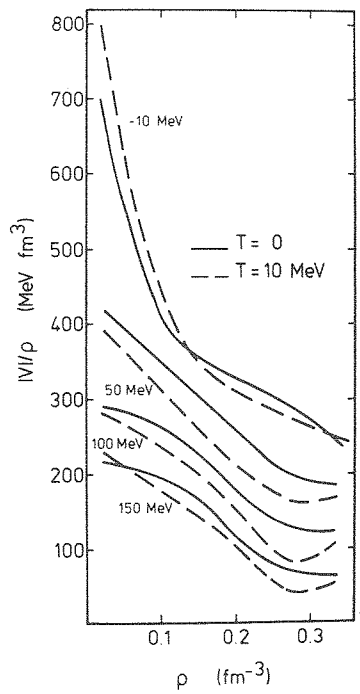

Fig. 11. Density and temperature dependence of the average effective interaction felt by a nucleon of energy E inside nuclear matter at density ρ, as defined by eq. (6.1). The numbers inside the figure give the energy E.

scattered inside the medium (see appendix A). We display this correlated wavefunction in fig. 12, restricting ourselves to a pair of nucleons in a relative s-state. More precisely, we consider the following quantity

$$\bar{u}(r) = \tfrac{1}{4}u^{1}{}_{S_0} + \tfrac{3}{4}u^{3}{}_{S_1}, \tag{6.2}$$

where the average has been taken on the spin states. The functions u are for an average value k_0 of the relative wave number (on the distribution $n(k)$). See appendix A for a precise definition of u. Also, in fig. 12, the defect function $\bar{\eta}(r)$

$$\bar{\eta}(r) = j_0(k_0 r) - \bar{u}(r) \tag{6.3}$$

is shown. In this equation, j_0 is the spherical Bessel function and the same average as in eq. (6.2) is considered. For cold matter, $\bar{u}(r)$ and $\bar{\eta}(r)$ present a typical behaviour. The strong repulsion of the two-body potential at short distances is responsible for the vanishing of $\bar{u}(r)$ at $r = 0$. The minimum of the function $\bar{\eta}(r)$ around 2 fm comes from the attractive part of the nuclear forces. The correlations never extend (in practice) farther than ~3 fm. The correlation pattern in $\bar{\eta}$ does not change very much for the three densities considered here.

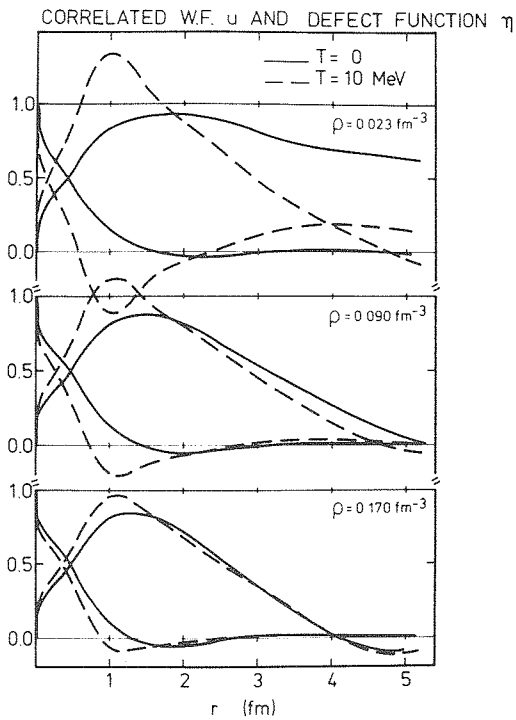

Fig. 12. Density and temperature dependence of the correlated wavefunction $\bar{u}$ and of the defect function $\bar{\eta}$ inside nuclear matter. See text for detail.

For a non zero temperature (here $T = 10$ MeV), the correlation pattern is sizeably changed. For all the cases considered here, the relaxation of the Pauli principle makes the repulsive forces less effective. This is akin with the temperature effect on the single-particle energies for low momenta: see discussion in sect. 4 and fig. 3. As a consequence, the function $\bar{\eta}$ possesses a well-defined minimum at a smaller distance than for cold matter. For finite temperature, the correlations extend at larger distances, because the two particles can really scatter. These correlations are not physical however. Indeed in an actual situation, these scattering correlations are expected to be destroyed by subsequent collisions with other partners. The connection between the function $\bar{\eta}$ and the two-body distribution functions or the related pair correlation function [39]) is not obvious. Note that these long-range correlations are not at all disturbing for all the considerations made here. The correlated wavefunction $\bar{u}(r)$ always occurs multiplied by the potential, which cuts the long-range part. The unphysical behaviour of $\bar{\eta}$ at large distance is linked to the underlying independent pair approximation inherent to Brueckner theory.

7. Discussion and conclusion

We have investigated various properties of cold as well as hot nuclear matter (in the region relevant to intermediate energy nucleus-nucleus collisions) in an approach inspired from Brueckner theory and using microscopic nucleon-nucleon forces.

For cold nuclear matter, our results are very close to those of Friedman and Pandharipande [10]). A microscopic two-body force (the Paris potential in our case, the v_{14} interaction in ref. [10])) is not sufficient to ensure proper saturation. The saturating properties can be improved by the introduction of long-range three-body forces. Although the details of the forces are sometimes different, the three-body force used here and the one used in ref. [10]) aim to describe the exchange of the lightest bosons between three nucleons, when one of these can be in an intermediate Δ-resonance state. The remaining lack of saturation, which can be, but not exclusively, attributed to the other three-body forces, is about the same in our work as in ref. [10]) (see fig. 1). In both works, proper saturation is achieved, by using a phenomenological ad hoc correction, supposed to account for these remaining effects.

It is gratifying to see that the variational approach of ref. [10]) and the Brueckner approach used here give about the same results, corroborating a tendency observed since many years. The variational approach can be extended (and has been extended) to larger densities, in contrast to the Brueckner theory, whose validity is expected to break down above $\rho \approx 3$–4 times ρ_0. The results of ref. [10]) and of this work are at variance with those of refs. [11,12]), where it is claimed that proper saturation can be achieved with a two-body interaction *alone* in a relativistic approach. We acknowledge that in this case, there is no need of adding any phenomenological term. However, the situation is far from clear. First, the relativistic treatment is not

free from approximations without which the numerical approach calculation would not be possible. Second three-body forces cannot be pushed away without justification, although the effect embodied by the three-body force of ref. [21]) may partially be included in the treatment of ref. [12]). On the other hand, our calculation does not include the three-body correlation diagrams, which are known to be attractive. However, their contribution is substantially reduced [41]) for a continuous choice of the single-particle potential, as in this work. Furthermore, the treatment of the three-body forces is far from satisfactory. First, we did not include the $\boldsymbol{L}\cdot\boldsymbol{S}$ term coming from ρ-exchange. This would probably improve the calculation. Second, as explained in ref. [18]), the introduction of the Δ-resonances should renormalize the two-body force itself, because of dispersion effects on this resonance when embedded into nuclear matter. The complexity of the whole problem of three-body forces and their relation to field theoretical approach are discussed at length in ref. [18]).

For hot nuclear matter, our work can be compared with those of refs. [8,9]), which are also based on the Brueckner approach. In ref. [9]), where the emphasis is put on the neutron gas, the Reid soft core NN interaction is chosen, but the self-consistency on the single-particle states $e(k)$ is avoided. Only the kinetic energy enters into the energy denominator of the Bethe–Goldstone equation. In ref. [8]), the double self-consistency is performed, but the impact of this work is somewhat limited, due to the use of a crude NN potential. Both refs. [8]) and [9]) neglect three-body forces. Since these works are by far numerically simpler than ours, they go further into the predictions of the usual thermodynamical properties of nuclear matter, like the isotherms and the isoentropes. The numerical complexity of our approach, as well as its somewhat limited precision due to necessary numerical differentiations (see eq. (3.21)) on a loose mesh does not allow us to state about possible significant differences between our works and refs. [8–10]). Such a possibility is very unlikely, since there is a converging bunch of various calculations indicating that uniform nuclear matter behaves like a van der Waals fluid.

The present work is very relevant as for the study of single-particle properties, since in this case we achieve a very good accuracy for the single-particle spectrum $e(k)$. We have extensively discussed the temperature and density dependence of $e(k)$ and of related quantities, as well as, from time to time, the energy dependence and the influence of three-body forces. For temperature of the order of 10 MeV, one should not have expected drastic changes (compared to $T=0$), since, most of the time, the relevant parameter is $\sim T/\varepsilon_F$, where ε_F is the kinetic Fermi energy. Sometimes, as in the entropy expansion, these parameters even enter with larger power. But, some kinematical circumstances (see the discussion on the mean free path in sect. 5.2) give rise to a change with respect to $T=0$, which is more drastic than indicated by the small parameter T/ε_F.

Let us emphasize our most important results:

(i) The real part of average single-particle potential $U(k)$ changes by a few percent, between $T=0$ and $T=10$ MeV, depending upon the density;

(ii) The imaginary part of $U(k)$ is drastically changed in the same temperature interval for low density. The modification is less and less important when the density increases;

(iii) This modification is due to the opening of the 2p-1h phase-space accessible by a nucleon of momentum k and to the dynamical change of the g-matrix coming from the "heating" of the Pauli principle. The second effect may be as important as the first one. We want to contrast this result with the recent work of ref. [42]), which treats the same problem, but using a model energy-independent effective interaction. As for the phase-space effects, our result and ref. [42]) grossly agree with each other;

(iv) The intrinsic non locality of the mean field (the one coming from the k-dependence of the mass operator) decreases when the matter is heated and when the density decreases;

(v) There is an important temperature effect on the effective mass. The peak above the Fermi level, at $T=0$, due to core polarization effects, rapidly collapses as the matter is heated;

(vi) The failure of Hartree-Fock calculations to reproduce the level density parameter is interpreted as coming from a too small effective mass ($\approx 0.7\ m$) at the Fermi level. We argued that single-particle estimates of the entropy is inappropriate because of the same reason;

(vii) We exhibited the temperature and density dependence of the nucleon mean free path inside nuclear matter. Here also, our calculation incorporates phase-space effects as well as dynamical effects linked with the heating of the Pauli principle and non locality effects (presence of $\tilde{m}$ in eq. (5.11)). Again, our results should be compared with previous works. In ref. [42]), the mean free path is calculated without the second effect. In ref. [43]) (for $T=0$ only), the Pauli principle is treated on a simple manner as in the old work of ref. [44]) and the non locality is neglected.

We also investigated the temperature dependence of the pair correlations as depicted by the NN correlated wavefunction. The correlation due to the attractive interactions are more and more important as the matter is heated. This introduces a word of caution for our treatment of the three-body force. In this work, the latter is "frozen", whereas the modification of the correlation induces a modification of the three-body force. A rough estimate indicates that the latter could be changed by 10–20% during heating from 0 to 10 MeV.

Finally, we have studied the temperature dependence of effective interaction. This question is of great actuality since many Hartree-Fock or related calculations are done at various temperatures with a frozen interaction. Our results more or less justify these procedures, since we have found a modification of a few percent only for an increase in temperature from 0 to ~20 MeV. This is a global description of the effective interaction however, which should be refined in view of the many parameters that characterize the states of the interacting nucleons. We want to stress this result, since it is the first unambiguous answer to this question. Previous works [8,14]) have addressed to the same question, but as we said, their conclusion,

the same as ours, was sometimes taken with some skepticism, because of the simplified treatment. Furthermore, these works were devoted to neutron matter.

We are very grateful to the FNRS Belgium, for the opportunity of using a CRAY-XMP computer. One of us (A.L.) would like to thank very much the CRN Strasbourg for the kind hospitality extended to him.

Appendix A

BETHE-GOLDSTONE INTEGRAL EQUATION FOR A VELOCITY DEPENDENT POTENTIAL

The general approach to the nuclear matter problem adopted here is the one followed by the Liège group [15]). The basic equation is the Bethe-Goldstone integral equation for the correlated wavefunction Ψ which for a velocity dependent potential can be written as

$$\Psi(\boldsymbol{k}, \boldsymbol{r}) = \chi(\boldsymbol{k}, \boldsymbol{r}) + \int \mathrm{d}^3 r'\, G_k^{(+)}(\boldsymbol{r}, \boldsymbol{r}')\, V(\boldsymbol{r}', \nabla')\, \Psi(\boldsymbol{k}, \boldsymbol{r}')\,, \tag{A.1}$$

where ∇' acts on $\boldsymbol{r}'$, $\chi(\boldsymbol{k}, \boldsymbol{r})$ stands for a plane wave and $\boldsymbol{k}$ is the relative momentum of the interacting pair. The Green function includes the proper boundary conditions and corresponds to the propagator in eq. (2.2). After the usual angle average is done [16]) in the Green function, the orientation of the vector $\boldsymbol{k}$ is irrelevant. A partial wave expansion can be performed both on χ and Ψ. Tensor forces couple different partial waves. For the sake of the clarity of the presentation, we disregard here this coupling.

In the l partial wave, the Green function $G_{l,k}^{(+)}$ can be written as

$$G_{l,k}^{(+)}(r, r') = \frac{1}{2\pi^2}\left\{ \mathscr{P} \int_0^\infty \frac{k'^2\, \mathrm{d}k'\, j_l(k'r) j_l(k'r') \bar{f}(k')}{\tilde{D}(k')} - i\pi k_0^2 j_l(k_0 r) j_l(k_0 r') \bar{f}(k_0) |D'(k_0)|^{-1} \right\}, \tag{A.2}$$

where $\mathscr{P}$ stands for the principal value of the integral and where j_l is the spherical Bessel function. In eq. (A.2), $D(k')$ represents the angle averaged energy denominator [16]) appearing in eq. (2.2). It implies the total momentum of the interacting pair. The quantity $\tilde{D}(k')$ is the real part of $D(k')$, obtained by dropping $i\varepsilon$. Finally, k_0 is the root of the denominator $\tilde{D}(k) = 0$, $D'(k)$ is the derivative of $D(k)$ and $\bar{f}(k')$ is the angle averaged Pauli operator (see appendix B). We have adopted here the method of ref. [27]) to take care of the principal value integral. An alternative method can be found in ref. [40]).

For the Paris potential, in any of the spin-isospin state, the potential writes

$$V(\boldsymbol{r}, \nabla) = V^0(r) - \frac{\hbar^2}{2m}[\nabla^2 V^b(r) + V^b(r)\nabla^2]\,. \tag{A.3}$$

The second derivatives are a source of trouble and we checked that they give rise to numerical instabilities when eq. (A.1) is solved as is, by standard techniques. The idea here is to perform by parts the integration involving the V^b terms. Use is made of the differential equation obeyed by the Green function $G^{(+)}_{l,k}(r, r')$

$$\left[\frac{1}{r'^2}\frac{\partial}{\partial r'}r'^2\frac{\partial}{\partial r'}+k_0^2-\frac{l(l+1)}{r'^2}\right]G^{(+)}_{l,k}(r, r')=-\frac{k_0}{2\pi}|D'(k_0)|^{-1}\frac{\delta(r-r')}{r^2}+H_l(r, r') \qquad (A.4)$$

with

$$H_l(r, r')=-\frac{1}{2\pi^2}\int_0^\infty j_l(kr)j_l(kr')[\bar{f}(k)-1]k^2\frac{k^2-k_0^2}{\bar{D}(k)}\,dk. \qquad (A.5)$$

The quantity $k_0/|D'(k_0)|$ in front of the δ-function arises because the denominator contains single-particle energies $e(k)$, which are more general than the quadratic law for noninteracting particles. The quantity $H_l(r, r')$ comes because the Green function used here contains the Pauli operator. The l-wave part of eq. (A.1) can, by this way, be written as

$$\left[1+\frac{8\hbar^2}{2m}\frac{k_0}{|D'(k_0)|}V^b(r)\right]u_{l,k}(r)$$
$$=j_l(kr)+4\pi\int_0^\infty dr'r'^2\left\{\left[G^{(+)}_{l,k}(r, r')V^0(r')-4\left(\frac{\hbar^2}{2m}\right)V^b(r')H_l(r, r')\right]u_{l,k}(r')\right.$$
$$\left.+4\frac{\hbar^2}{2m}\frac{dV^b(r')}{dr'}G^{(+)}_{l,k}(r, r')\frac{du_{l,k}}{dr'}(r')\right\}, \qquad (A.6)$$

The general expression, when tensor forces are present, can easily be guessed, as well as the relation between the functions V^0 and V^b and the usual parametrization of the Paris potential [13]).

As shown by eq. (A.6), we have eliminated the second derivative of u, but we are left with the first derivative. The latter cannot be avoided since an integration by parts of the last term in eq. (A.6) would involve the derivative of the Green function which is even worse. The derivative of u is evaluated by a four point Lagrange formula, after discretization. Eq. (A.6) is solved by matrix inversion. Typically, the r' integration is performed by the Chebyshev integration method in the intervals 0–0.133, 0.133–0.321, 0.321–0.686, 0.686–2.05 fm with respectively 7, 4, 7 and 5 points. A modified Gauss integration formula with 7 points is retained for $2.05 \leq r \leq$ 12 fm. Check of the numerical procedure is done by recovering the NN phase shift (no Pauli operator, pure kinetic energy in the single-particle energy, very low density). An integration on r is required to go from the correlated function u to the g-matrix element [16]). The same mesh is used as for eq. (A.6).

Evaluation of $U(k)$, eq. (2.5), involves an integration on the momentum j and on the angle between k and j. The standard method of ref. [16]) is used for the angle, but much more integration points than in refs. [16,27]) are used for j, since now the

function $n(j)$ is more rapidly varying (for $T \neq 0$). Limiting l and the total angular momentum J to 5, a full calculation of $U(k)$ for a given k takes 5 to 15 seconds on a CRAY-XMP computer, depending on the number of points in j, for a single iteration. In general, about 6 iterations are required to reach an acceptable self-consistency. The whole calculation required 2h45min of CRAY-XMP computer CPU time.

Appendix B

"HEATED" PAULI OPERATOR

In the absence of average potential, the Pauli operator (2.3) at $T \neq 0$ can be written as

$$Q(a, b) = \frac{1}{1+\exp[A+B\cos\vartheta]} \frac{1}{1+\exp[A-B\cos\vartheta]}, \tag{B.1}$$

where

$$A = \beta\mu + \frac{\beta\hbar^2}{2m}(k^2+\tfrac{1}{4}P^2), \qquad B = \frac{\beta\hbar^2}{2m} kP, \tag{B.2}$$

k and P being the relative and total momenta respectively, and ϑ being the angle between k and P. The angle average over ϑ can be performed analytically (by the substitution $y = \exp(Bx)$), yielding

$$\begin{aligned} \bar{f} &= \tfrac{1}{2}\int_{-1}^{1} \mathrm{d}x \frac{1}{1+\exp[A+Bx]} \frac{1}{1+\exp[A-Bx]} \\ &= \frac{1}{1-\exp(2A)} \times \left[1 - \frac{2m}{\beta k P \hbar^2} \ln \frac{1+\exp(A-B)}{1+\exp(A+B)}\right]. \end{aligned} \tag{B.3}$$

For a single-particle spectrum $e(k)$ which is not quadratic in k, the analytical integration (B.3) is no longer possible. Here, we took advantage of the almost quadratic law for all the k-values of interest. For $0 < k < 1.5k_F$, we have fitted at each time of the calculation $e(k)$ by

$$e(k) \approx e_0 + ak^2. \tag{B.4}$$

In this case, (B.3) remains valid after the substitution $\hbar^2/2m \to a$, $\mu \to \mu - e_0$.

References

1) J. Cugnon, Dynamics of the relativistic heavy ion collisions, Lectures at the Cargèse Summer School, 1984 (Plenum) to be published
2) H. Stöcker and W. Greiner, preprint MSUCL-540, Phys. Reports, to be published
3) I. Mishustin, Proc. of the Visby Conference, Nucl. Phys. **A447** (1986) 67c
4) P. Bonche, S. Levit and D. Vautherin, Nucl. Phys. **A427** (1984) 278
5) J. Hüfner, Phys. Reports **125** (1985) 129

6) M. Brack and P. Quentin, Phys. Lett. **52B** (1974) 159
7) G. Röpke, L. Münchow and H. Schultz, Phys. Lett. **110B** (1982) 21
8) J.R. Büchler and S.A. Coon, Astrophys. J. **212** (1977) 807
9) R.M. Tripathi, Phys. Rev. **C25** (1982) 1114
10) B. Friedman and V.R. Pandharipande, Nucl. Phys. **A361** (1981) 502
11) M.R. Anastasio, L.S. Celenza, W.D. Pong and C.M. Shakin, Phys. Reports **100** (1983) 327
12) R. Machleidt and R. Brockmann, Phys. Lett. **160B** (1985) 364
13) M. Lacombe *et al.*, Phys. Rev. **C21** (1980) 861
14) J.R. Büchler and B. Datta, Phys. Rev. **C19** (1979) 494
15) J.-P. Jeukenne, A. Lejeune and C. Mahaux, Phys. Reports **25C** (1976) 85
16) K.A. Brueckner and J.L. Gammel, Phys. Rev. **109** (1958) 1023
17) B.D. Day, Comm. Nucl. Part. Phys. **11** (1983) 115
18) A.D. Jackson, Ann. Rev. Nucl. Part. Sci. **33** (1983) 105
19) A.D. Jackson, M. Rho and E. Krotscheck, Nucl. Phys. **A407** (1983) 495
20) J. Carlson, V.R. Pandharipande and R.B. Wiringa, Nucl. Phys. **A401** (1983) 59
21) M. Martzolff, B. Loiseau and P. Grangé, Phys. Lett. **92B** (1980) 46
22) B.A. Loiseau, Y. Nogami and C.K. Ross, Nucl. Phys. **A165** (1971) 601
23) M.A. Matin and M. Dey, Phys. Rev. **C27** (1983) 2356
24) D.J. Thouless, The quantum mechanics of many-body systems, 2d ed. (Academic Press, NY, 1972)
25) N.M. Hugenholtz and L. Van Hove, Physica **24** (1958) 363
26) J. Cugnon, Phys. Lett. **135B** (1984) 375
27) J.-P. Jeukenne, A. Lejeune and C. Mahaux, Phys. Rev. **C16** (1977) 80
28) J.W. Negele and K. Yazaki, Phys. Rev. Lett. **47** (1981) 71
29) S. Fantoni, B.L. Friman and V.R. Pandharipande, Phys. Lett. **104B** (1981) 89
30) C. Mahaux, Phys. Rev. **C28** (1983) 1848
31) M. Jaminon, C. Mahaux and P. Rochus, Phys. Rev. Lett. **43** (1979) 1077
32) P.E. Hodgson, Nuclear reactions and nuclear structure (Clarendon, Oxford, 1971)
33) A.L. Fetter and J.D. Walecka, Quantum theory of many-particle systems (McGraw Hill, NY, 1971)
34) R. Sartor and C. Mahaux, Phys. Rev. **C21** (1980) 1546
35) G.E. Brown, J.H. Gunn and P. Gould, Nucl. Phys. **46** (1963) 598
36) G. Bertsch, Progress in particle and nuclear physics, vol. 4, ed. D. Wilkinson (Pergamon, Oxford, 1980)
37) H.A. Bethe, Phys. Rev. **167** (1968) 879
38) N. Yamaguchi, S. Nagata and T. Matsuda, Prog. Theor. Phys. **70** (1983) 459
39) R. Balescu, Equilibrium and nonequilibrium statistical mechanics (Wiley, NY, 1975)
40) L. Rikus, N. Nakano and H.V. von Geramb, Nucl. Phys. **A414** (1984) 413
41) P. Grangé and A. Lejeune, Nucl. Phys. **A327** (1979) 335
42) A.H. Blin, R.W. Hasse, B. Hiller and P. Schuck, Phys. Lett. **161B** (1985) 211
43) N.J. DiGiacomo, R.M. De Vries and J.C. Peng, Phys. Rev. Lett. **45** (1980) 527
44) K. Kikuchi and M. Kawai, Nuclear matter and nuclear reactions (North-Holland, Amsterdam, 1968)